Papaver rhoeas L. Mapping with Cokriging Using UAV Imagery

Montserrat Jurado-Expósito[1], Ana Isabel de Castro, Jorge Torres-Sánchez, Francisco Manuel Jiménez-Brenes and Francisca López-Granados

Institute for Sustainable Agriculture, CSIC, 14004 Córdoba, Spain

[1]Montserrat Jurado-Expósito

e-mail: montse.jurado@ias.csic.es,

Phone: + 34 957 499 363

ORCID: 0000-0003-2796-0565

Acknowledgments

This research was financed by the AGL2014-52465-C4-4-R and AGL2017-83325-C4-4-R MINECO (Spanish Ministry of Economy and Competition, FEDER Funds). Research of AI. de Castro was financed by Juan de la Cierva (MINECO) program. The authors thank Dr. Recasens and his group for their valuable help in field surveys.

Abstract

Accurately mapping the spatial distribution of weeds within a field is a first step towards effective Site-specific Weed Management. The main objective of this study was to investigate if the multivariate geostatistical method of cokriging (COK) can be used to improve the accuracy of *Papaver rhoeas* L. infestations maps in winter wheat fields using high-resolution UAV imagery as ancillary information. The primary variable was obtained by intensive grid weed density field samplings and the secondary variables were derived from the UAV imagery taken the same day as the weed field samplings (e.g. wavebands and derivative products, such as band ratios and vegetation indexes). Univariate Ordinary Kriging (OK) and multivariate Cokriging (COK) interpolation methods were used and compared for Papaver density mapping. The performances of the different methods were assessed by cross-validation. The results indicated that COK outperformed OK in the spatial interpolation of Papaver density. COK reduced the prediction errors and enhanced the accuracy of Papaver estimates maps. The best performances were obtained when COK was performed with the UAV-secondary variables that yielded the highest correlation with Papaver density and produced the strongest spatial cross-semivariograms. On average, the COK with UAV-derived ancillary variables improved the accuracy of mapping Papaver density by 11 to 21% compared with OK. The results suggest the great potential of high-resolution UAV imagery as a source of ancillary information to improve the accuracy of spatial mapping of sparsely sampled target variables using COK.

Keywords Ancillary variables, Corn poppy, Geostatistic, Kriging, Precision Agriculture, cross-semivariogram, SSWM, Weeds.

Introduction

Precision Agriculture (PA) aims at managing natural resources and crop spatial and temporal variations to meet the actual site-specific needs of crops rather than the average needs of whole fields (National Research Council 1997; Zang et al. 2002). One of the main targets of PA is the improvement of crop production management with spatially variable within-field practices, which requires an accurate assessment of spatial variations at very fine scales of resolution, reducing inputs and maximizing outputs with the preservation of the environment (Yao and Huang 2013).

Site Specific Weed Management (SSWM) is an application of PA accounting for the within-field variability of weed infestation and applying weed management inputs based on site-specific variability (Christensen et al. 2009). Weeds are typically not uniformly distributed across fields and tend to appear in patches (Jurado-Expósito et al. 2003, 2009; Barroso et al. 2004; Gerhards and Christensen 2006). Accurately mapping the distribution of weeds within a field is a first step towards effective weed management. Patchy distribution mapping is necessary to prevent the spread of weeds to clean areas, which is particularly relevant for invasive or resistant weeds, and to implement SSWM only where weeds are located at densities greater than those that cause economic losses. To develop effective SSWM strategies based on maps, robust methods for weed data acquisition and analysis procedures that integrate knowledge about the density and spatial variability of infestations are required. Unfortunately, such information cannot be obtained solely from traditional survey techniques because weed sampling on the ground is generally time-consuming, labour-intensive and involves high costs. An alternative for predicting the spatial distribution of weeds is by the use of spatial interpolation techniques, such as geostatistics.

Geostatistics measures the spatial fluctuations of studied numerical variables based on rigorous sampling; the data are used to adjust a semivariogram model that defines the degree of spatial correlation between the data points and quantifies the spatial variability of variables via interpolation by kriging algorithms and the production of maps with different levels of the variable studied. A detailed presentation of the theory of applied geostatistics is

given in Matheron (1970), Isaaks and Srivastava (1989), Goovaerts (1997) and Webster and Oliver (2007).

Kriging is currently accepted by weed scientists as an appropriate technique for estimating weed infestations at unsampled sites. Through relatively simple procedures, it is possible to obtain maps with weed infestation locations and densities, resulting in an extremely valuable tool for deciding whether to apply a SSWM strategy based on whether weeds are present in a specific site or exceed the control threshold (Heisel et al. 1996; Oliver 2010). Although kriging has been widely used as an alternative to predict the spatial distributions of weed species (e.g. Donald et al. 1994; Cardina et al. 1997; Colbach et al. 2000; Dille et al. 2003; Jurado-Expósito et al. 2003; 2009; Barroso et al. 2005, Blanco-Moreno et al. 2006; Izquierdo et al. 2009 and Kalivas et al. 2012, among many others), researchers often have few sampled sites in relation to the area to be mapped and have reported that simple interpolation procedures sometimes perform poorly for weed mapping when the number of samples that are available is restricted, e.g., by economic constraints. To overcome this drawback, combinations of kriging with correlated densely sampled auxiliary variables have been suggested to enhance the accuracy of predictions for variables of interest (Goovaerts 1997; Wakernagel 2003; Webster and Oliver 2007). Among these procedures, cokriging (COK) is commonly used when the sampling for a variable of interest (primary variable) is poor, and other variables (secondary variables) are more densely sampled because they are easier or cheaper to measure, reducing the sampling costs and increasing the prediction accuracy of the sparsely sampled target variable (Isaaks and Srivastava 1989; Webster and Oliver 2007; Chilès and Delfiner 2012; Emery 2012). COK has been successfully used to improve weed mapping by using auxiliary variables correlated with weed density, such as soil properties (Heisel et al. 1999; Walter et al. 2002; Kalivas et al. 2012).

Cokriging is most beneficial where the variable of interest is less densely sampled than the other variables. This is clearly likely to be the case where the secondary variable is provided by remote sensing imagery that completely covers the region of interest. Remote

sensing offers an inexpensive means of deriving complete spatial coverage of environmental information for large areas at regular time intervals, and it can therefore be extremely useful in providing ancillary variables to estimate. Van Der Meer (2012) reviewed the state of the art of how geostatistics is used in remote sensing studies. Among others, COK has been used to link image data to ground data, i.e. to combine field and image data in a joint prediction of a field variable. COK is used to better estimate field variables by exploiting the correlation between image data (or derivative products, such as Vegetation indexes, e.g., NDVI) and field measurements (Van Der Meer 2012). Cokriging has been successfully used to combine ancillary data derived from satellite imagery or piloted airborne vehicles to e.g. map herbaceous biomass (Mutanga and Rugege 2006), provide better estimates of forest parameters (Meng et al. 2009; Hernández-Stefanoni et al. 2011) or estimate woody vegetation (Adjorlo and Mutanga 2013). However, airborne data are expensive and data from sensors on-board satellite platforms are often not suitable for weed mapping due to their low spatial and temporal resolutions. Therefore, more refined image acquisition with a higher spatial and/or spectral resolution might be necessary to be further exploring this technique that combines weed sampling and remote sensing data to improve the mapping accuracy for the implementation of SSWM strategies.

Currently, there are other remote platforms, the Unmanned Aerial Vehicles (UAV), that can generate data with a high spatial-resolution. Research on the use of UAVs in the context of precision agriculture has increased considerably in recent years (Zhang and Kovacs 2012; Huang et al. 2017). The main advantages of using UAVs are that they can carry different sensors to record reflected energy at diverse spectral ranges in accordance with detection objectives, fly at different altitudes to adjust the desired spatial resolution and be programmed on demand at critical stages of crop growth (Torres-Sánchez et al. 2013). There is a growing interest in the agricultural community in using UAVs as a decision support tool for PA applications, including SSWM (Rasmussen et al. 2013; Castaldi et al. 2017). Huang et al. (2017) have published an overview about the development and applications of UAVs at low altitudes for precision weed management, and the potential of UAVs for

mapping weeds at field scales has been recently evaluated by Lambert et al. (2018). UAV images have been successfully used to detect and map broadleaved and grass weeds patches within annual crops for early postemergence SSWM programs (Peña et al. 2013; Castaldi et al. 2017; Lottes et al. 2017; Torres-Sánchez et al. 2014, López-Granados et al. 2016; Barrero and Perdomo 2018). This increasing development and use of UAVs provides a quick, timely and economical source of ancillary information that can be used to enhance the accuracy of estimations, however, so far, the use of kriging with UAV-derived auxiliary variables to improve the spatial mapping of a sparsely sampled variable is rare (Schirrmann et al. 2017). There are just a few applications in soil science and environmental science. In precision agriculture, only one recent study has used regression kriging in combination with UAV imagery to develop crop height models for wheat fields (Schirrmann et al. 2017). Thus far, the combination of COK with secondary information from high-resolution UAV imagery has not been used to improve the spatial mapping of weeds.

Papaver rhoeas L. (corn poppy) is the most important broad-leaved weed specie infesting dry-land winter cereals in areas of southern Europe with a Mediterranean climate (Wilson et al. 1995). Because of its high seed production, highly persistent seeds and extended period of germination, Papaver is difficult to control; furthermore, it is a very competitive weed that can substantially reduce grain yields up to 32% (Holm et al. 1997; Torra and Recasens 2008). In the last two decades, this situation has worsened because of the recent development of herbicide-resistant populations. In Spain, resistant populations are particularly abundant in the northeast region of the country, with biotypes resistant to 2,4-D and tribenuron-methyl (Taberner et al. 2001; Torra et al. 2010). Farmers have become increasingly concerned about herbicide-resistant Papaver since they are not able to achieve good control of the resistant populations using herbicides alone, so the introduction of alternative SSWM strategies integrating herbicide and non-herbicide tactics is required (Torra et al. 2008). These tactics should be specifically designed and tested for each region, especially in Spanish dry land areas where cereal yields are low and alternative crop options to cereals are very limited (Cantero-Martínez et al. 2007). As state above, the efficiency of a

SSWM system strongly depends on the accuracy of the weed map, in this context, to develop SSWM strategies for Papaver an accurate assessment and a complete knowledge of weed spatial variability within fields at very fine scales of resolution are required.

Considering the factors introduced above, the main objective of this study was to investigate if the multivariate geostatistical method of cokriging can be used to improve the accuracy of Papaver infestations maps in winter wheat fields using UAV imagery data (wavebands and derivative products, such as band ratios and vegetation indexes) as secondary variables. As far as the authors of this paper know, this is the first approach to weed mapping via UAV imagery combining spectral information and multivariate geostatistical analyses. This methodology is expected to contribute significantly towards the enhanced accuracy weed mapping for the implementation of SSWM strategies for Papaver.

Materials and Methods

Study site and weed sampling

The study was conducted in five commercial winter wheat fields located in the provinces of Lleida (Baldomar, Boix and Muller) and Córdoba (Cañaveral Norte and Cañaveral Sur), typical agricultural areas in Catalonia (north-eastern Spain) and Andalusia (southern Spain), respectively. Fields were chosen because local farmers had reported poor Papaver control with 2,4-D and/ or tribenuron-methyl. All fields were farmer-managed and the typical agronomic practices for the regions were used. Papaver was the main broad-leaved weed in all five fields with no other problematic species, so no additional herbicides were applied.

The primary variable (i.e. Papaver density, which is the target variable of study) was obtained by intensive grid field surveys conducted in selected areas within the larger fields and their borders were at least 20 m from the main borders of the fields. The surveys were conducted when the winter wheat showed the typical green-yellow colour of the beginning of the maturation stage and Papaver weed patches displayed an intensive red-purple colour corresponding to the flowering growth stage. Weed assessments were performed following a 10 m by 10 m grid pattern. Details of sampled areas and the resulting sampled sites in each

field are shown in Table 1. The position of each node was georeferenced using a Trimble Geo-XH Differential GPS (DGPS) and the total number of Papaver plants was recorded at the grid points in 1 m^2 squares.

UAV image acquisition and processing

The secondary information was derived from the UAV images taken the same day as the weed field samplings. A model MD4-1000 quadrocopter UAV (microdrones GmbH, Siegen, Germany) with the capacity to carry any sensor weighing less than 1.25 kg mounted under its belly and flight autonomy of 45 minutes was used to collect the remote images. This model, with vertical take-off and landing capabilities, can fly either by remote control or autonomously with the aid of its GPS receiver and its waypoint navigation system. Two sensors with different spectral and spatial resolutions were separately mounted on the UAV in the studies: a still point-and-shoot camera model Olympus PEN E-PM1 (Olympus Corporation, Tokyo, Japon) and a modified, commercial, off-the-shelf camera, model Sony ILCE-6000 (Sony Corporation, Tokyo, Japan). The Olympus camera takes 12 megapixel (4,032 x 3,024 pixels) images in true colour (Red, R; Green, G; and Blue, B, wavebands). The camera´s sensor size is 17.3*13 mm and the pixel size is 0.0043 mm. (Torres-Sánchez et al. 2013). The Sony camera acquires 24 megapixel images (6,000 x 4,000 pixels) images, and was modified to capture information in both near-infrared (NIR) and visible light (G and R). The modification consisted in the removal the internal NIR filter from the camera (present in all RGB digital camera sensors) and the application of an external 49-mm filter ring to the front nose of the lens to avoid the blue light reaching the sensor in order to store the NIR information in the blue channel of the images. The camera was modified by Mosaicmill (Mosaicmill Oy, Vantaa, Finlandia) where a focus calibration process was carried out. The camera´s sensor size is 23.5 x 15.6 mm and the pixel size is 0.0039 mm (De Castro et al. 2018).

The UAV images were collected at a flight altitude of 120 m, which complies with the requirements established by the Spanish National Agency of Aerial Security, with a

transverse overlap of 60% and a longitudinal overlap of 90%, thus allowing the generation of quality ortho-mosaicked images, according to previous research (Torres-Sánchez et al. 2013; Mesas-Carrascosa et al. 2015, 2017). The flight routes for each camera were programmed and automated, and only the take-off and landing were manually performed by the pilot. A set of artificial ground control points (GCP) consisting of a square card numbered with a cross marked, so that it can be seen clearly in the images, were placed in the fields and geo-referenced using a DGPS to obtain the GCPs coordinates to perform the imagery orthorectification and mosaicking process. In the course of the UAV flights, a 1 x 1 m barium sulphate standard Spectralon® panel (Labsphere Inc., Norht Sutton, NH, USA) was also placed in the middle of the fields to calibrate the spectral data.

The orthomosaics were generated using Agisoft PhotoScan Professional Edition software (Agisoft LLC, St. Petersburg, Russia). The software, with the exception of the manual localization of the GCPs to georeferenced the images, automatically performs the orthorectification and mosaicking of the imagery set into a single image of the whole experimental field (Fig. 1). The images taken flying at 120 m altitude produce RGB and RGNIR ortho-mosaicked images of 0.0368 and 0.0235 m/pixel of ground sampling distance (GSD), respectively. Detailed information on the configuration of the UAV flights, camera sensors specifications and image pre-processing (georeferencing, calibration, orthorectification and mosaicking processes) can be found in Torres-Sánchez et al. (2013), Mesas-Carrascosa et al. (2015, 2017) and De Castro et al. (2018).

The georeferenced sampling points from field surveys were identified and located in the corresponding ortho-mosaicked; then were assigned to one of classes considered in the study (i.e., Papaver weeds and winter wheat) based on the information provided by the on-ground field sampling; and its digital values in blue (B), green (G), red (R) and near-infrared (NIR) waveband were extracted. In addition to the four wavebands, four band ratios and nine vegetation indexes derived from wavebands were calculated (Table 2). ENVI 5.0 software (Research Systems Inc., 2012) was used to extract the digital data and to calculate the band

ratios and vegetation indexes. These 17 variables derived from UAV imagery were used as ancillary data in the subsequent multivariate analyses.

Geostatistical analysis

The geostatistical analyses started with the exploratory analysis of the primary variable (Papaver density). For each field, the weed density data were treated as a study case, and classical descriptors, such as the mean, maximum, standard deviation and skewness, among others, were determined. Particular attention was given to the statistical distribution of the primary variable because departures from normality affect the stability of variances and, consequently, the semivariogram. Similarly, the mean and standard deviation of the 17 UAV-derived ancillary variables were calculated and the Kolmogorov–Smirnov test was performed on all digital data sets to verify that all secondary variables were normally distributed. Pearson's linear correlations were determined between the Papaver density and UAV digital values to assess the relationships between weed density and the UAV-derived ancillary variables. The wavebands, band ratios or vegetation indexes that yielded the highest significant correlation with weed density will be used in a multivariate geostatistical analysis to estimate Papaver density for the whole winter wheat fields.

The spatial variability of Papaver in each winter wheat field was described by a semivariogram that express the spatial dependence between the weed density at different separation distances and directions, whereas kriging and cokriging were used to interpolate and map Papaver density. Experimental semivariograms were computed for each variable using ArcGIS 10.1 (Geostatistical Analyst module, 10.1). Potential directional trends in the spatial distribution of weed density were checked by calculating the experimental semivariograms both isotropically and anisotropically. The anisotropic calculations were performed in four directions (0, 45, 90, and 135°) with a tolerance of 22.5. Several semivariograms functions were evaluated to choose the best fit with the data. Spherical and exponential models were fitted to the experimental semivariograms and the parameters of the model (i.e. range, nugget and sill) were determined. The least-square fit procedure in

ARCGis 10.1 (Geostatistical Analyst module, 10.1) was used both as the criterion to select the best model and to fit the experimental semivariograms. In addition, to define the degree of spatial dependence of the Papaver density, the nugget variance expressed as the percentage of the total semivariance or sill, i.e., the Spatial Dependence index (SD) was calculated. SD values close to zero (≤ 25%) indicate a variable strongly spatially dependent or strongly distributed in patches, and SD values close to 100 (≥ 75 %) indicate a variable weakly spatial dependent (Cambardella and Karlen 1999).

Semivariograms models were cross-validated to check the validity of the models and to compare values estimated from the semivariogram model with the actual values (Isaaks and Srivastava 1998; Goovaerts, 2000). The cross-validation was assessed by Leave-One-Out (LOO-CV) procedure using the geostatistical analysis tool for ArcGIS (Geostatistical Analyst module, 10.1). One weed density observation was temporarily removed at a time from the data set, and then predicted from remaining weed density data by either kriging o cokriging procedure mentioned in the following section. This procedure was repeated for all observations of the weed density in each field. Validation errors were the differences between the observed and the estimated values using the OK or COK method, and were assessed and compared using the following cross-validation statistics: 1) the mean estimation error (MEE), which is a bias indicator of the prediction, and must not significantly different than zero for unbiased methods; 2) the mean squared error (MSE) which must be small and less than the variance of the sample values (Hevesi et al. 1992) and 3) the standardized mean squared error (SMSE) which must be within the interval of $1 \pm 2\sqrt{2/n}$, where n is the number of observations (Isaaks and Srivastava 1989; Hevesi et al. 1992; Goovaerts, 2000; Webster and Oliver, 2007). Once cross-validated, the parameters of the semivariograms models were used to interpolate Papaver density by using two spatial estimation procedures: Ordinary Kriging (OK) and Cokriging (COK) on a regular grid of 0.5 m using the geostatistical analysis tool of ArcGis 10.1.

Ordinary kriging is the most commonly used type of univariate geostatistical algorithm to spatial estimation in weed science and the accuracy of kriged estimates depends on the

fitted semivariogram model. Cokriging is an extension of OK method, so as to improve the estimation of a studied variable (i.e. the primary variable, Papaver density in this case) by using information on other more densely recorded ancillary variables which are spatially correlated to the first one (in this study wavebands, band ratios and vegetation indexes derived from UAV imagery). To estimate the primary variable COK requires the estimation of the direct and cross-semivariogram models for the primary and the secondary variables. Experimental semivariograms were modelled for Papaver density and the ancillary variables separately, as well as the cross-semivariograms for all pairs of UAV-derived ancillary data and weed density measured at the same location. Several cross-semivariogram functions were evaluated to choose the best fit with the data, and LOO-CV was used to final selection of cross-semivariogram models for the multivariate spatial estimation of Papaver density. Cokriging was performed with the UAV-derived ancillary data that showed a strong correlation with weed density.

The last step of the geostatistical analysis was to construct the spatial distribution maps of Papaver density based on the ordinary kriged and cokriged (with wavebands, band ratios and vegetation indices) estimates.

Assessments of predictions methods

The predictive performance of spatial interpolation methods is usually evaluated with a cross-validation test (LOO-CV) by using prediction errors (Goovaerts, 2000). Several cross-validation statistical error measures have been proposed as a measurement of prediction quality to evaluate the goodness of spatial estimation approaches. Of the many possible numerical calculations on model residuals, by far the most common is Mean Square Error (MSE) criterion which squares the residuals before calculating the mean, making all contributions positive and penalizing greater errors more heavily (Bennett et al., 2013; Li and Heap, 2011). In this study, the performance of the OK approach was compared with that of different approaches that combine UAV remotely sensed data (wavebands, band ratios and vegetation indexes) and multivariate geostatistical models (COK) for predicting Papaver

density, by using the MSE of OK which did not consider the ancillary data, as the standard. For each prediction method, the MSE was calculated as an overall indication of the map precision quality. MSE should be close to zero if the algorithm is accurate, otherwise the prediction method would be worse than predicting Papaver density by the overall mean equally at all locations, and smaller MSE values indicate higher accuracy than larger values.

Results and Discussion

Exploratory Statistical Analysis

The exploratory analysis of the data revealed considerable spatial variation in the Papaver density among fields and a generally biased distribution of the data (Table 2). Cañaveral Sur, with a mean of 10.42 plants m^{-2}, was by far the field with the highest density values. In Baldomar, Boix and Muller Papaver was present at moderate density (5.3, 4.8 and 4.2 plants m^{-2}, respectively), and at a low density in Cañaveral Norte (2.9 plants m^{-2}). The values of skewness (> +1) indicated that weed density did not follow a normal distribution, and therefore, data were logarithmically transformed after a constant value of 1 was added to stabilize the variances and approximately normalize the data prior to estimating weed density, following the methodology described by Kerry and Oliver (2003). The skewness values of transformed data were between -0.339 to 0.571 (Table 2) indicating that the transformed variables were normally distributed and allowing all the successive procedures of variography and prediction. The results of the test of normality performed on digital data sets revealed that the 17 ancillary variables were normally distributed, and therefore, data were not transformed.

The relationships between Papaver density and UAV individual wavebands, band ratios and vegetation indexes are shown in Table 3. Most of secondary variables were correlated, though not to the same extend. In most of the field, the results showed a strong correlation between weed density and G waveband, B/G band ratio and ExG, ExG(2) and ExGR vegetation indexes (r values greater than |0.5|). Papaver density was moderately correlated with the B and R wavebands; the R/G and R/B band ratios and NGRDI, ExR and

ExR(2) vegetation indexes (|0.20| < r < |0.50|), and weakly correlated with NIR, NIR/G, RVI, NDVI and DVI (r ≤ |0.20|) (Table 3). Previous studies have suggested that low correlation coefficients observed for vegetation indexes, such as NDVI, can be attributed to the asymptotic nature of the NDVI–vegetation relationship as the growing season progresses (Tucker 1977; Kumar et al. 2001; Mutanga and Rugege, 2006). The problem of asymptotic saturation of vegetation indices is common with satellite multispectral imagery, and is particularly true for grassland or agricultural imagery (Tucker 1977). As the growing season progresses and vegetation increases, NDVI becomes saturated at dense vegetation levels, thus yielding low correlation coefficients with vegetation during the peak of the season, in areas where there is 100% vegetation cover (Thenkabail et al .2000). As the correlation increases, the information provided by the secondary variable to the primary variable increases, so stronger correlations will result in more accurate estimations of multivariate geostatistics (Goovaerts, 1997). The multivariate approach was performed by using the UAV-derived ancillary data that yielded a strong-moderate correlations with weed density (e.g. r > |0.20|).

The directional experimental semivariograms did not visually showed trends, and all exhibited almost the same range and sill, indicating the absence of anisotropy, so omnidirectional isotropic semivariogram models were fitted to the experimental simple and cross-semivariograms. Nested semivariogram structures were not used, since adequate fits could be obtained with a simple structure. The exponential model was the best fitted to the experimental simple semivariograms in all the fields (Fig. 2). Most of the variation was spatially correlated, with zero or low nugget component indicating that the sampling intervals were appropriated and no further sampling on a finer spatial scale was needed. Simple isotropic models without nugget were defined in four of the fields, and the remaining field had a low nugget value (Muller). The fitted semivariogram model parameters and the spatial distribution characteristics of Papaver density for each field are provided Table 4. Papaver density displayed differences in spatial dependence among the fields, and a similar variation was observed for the semivariogram parameters. The range varied among the fields with

values ranging from 15.44 m in Boix to 30.74 m Baldomar (Table 4) confirming that the sample grids were large enough to determine the spatial variability range for Papaver density and appropriate for the field surveys. The sill values also varied among fields, with values ranging from 0.65 to 1.23 in Cañaveral Sur and Baldomar, respectively. The nugget was zero in all fields studied, except for in Muller, where the nugget value was 0.375 (Table 4).

Low SD index values indicating a variable strongly spatially dependent or strongly distributed in patches were found in all locations, except for Muller, which presented a medium SD index (47.52%), indicating a moderate spatial dependence (Table 4). Due to the strong spatial structuring of Papaver density (SD ≤ 25%), choosing geostatistical methods for interpolation should be reasonable and beneficial, as the spatial structure inherent to the density data set can be well implemented with the semivariogram models in the interpolation methods.

The cross-validation results for the five fields confirmed that the fitted simple semivariogram models for Papaver density satisfy the cross-validation conditions (Table 4) and were thus suitable for the OK interpolation.

Isotropic experimental cross-semivariograms were also fitted well by the exponential model with or without nugget, depending on the field and ancillary variable considered. The secondary variables that were more highly correlated with Papaver density also produced better-structured cross-semivariograms (Journel and Huijbregts 1978), e.g., cross-semivariograms for Papaver density and the G waveband, B/G and R/B band ratios and ExG, ExR, NGRDI, ExG(2) ExR(2) and ExGR Vegetation indexes (Figure 3). The fitted cross-semivariogram model parameters and their cross-validation results for each field are provided in Table 5. As shown by these figures, the values of the experimental cross-semivariogram increased over distances from 0 to 25 m (more than half of the maximum sampling distance) for most of the secondary variables, indicating that a positive spatial cross-correlation existed between the Papaver density and ancillary data derived from UAV imagery. The range and the sill of the cross-semivariograms models vary from one field to another, but they were similar for a given field regardless of the secondary variable

considered. The cross-validation statistics also varied from one secondary variable to another and among the fields (Table 5) but adequate cross-validation results were obtained for all cross-semivariogram models, indicating that the adopted cross-semivariograms models would be suitable for COK analysis. Among the secondary variables that produced the better-structured cross-semivariograms (Figure 3) only those UAV-derived variables more highly correlated with Papaver density (i.e. $r > |0.50|$) were considered for COK; that is G waveband, B/G band ratio and ExG, ExG(2) and ExGR vegetation indexes.

Kriging and cokriging values were transformed back to the original scale in order to create the spatial distribution maps of Papaver density in the five winter wheat fields. The weed density maps produced with OK and COK estimates on a regular grid of 0.5 m are shown in Figures 4 and 5, respectively. A visual assessment reveals a strongly to moderately patchy distribution of Papaver density which was also supported by the semivariogram analyses (Table 4). In general, the weed density patterns in the cokriged maps are similar to those in the OK maps (Fig.4). Visual discrepancies existed between the cokriged maps based on the ancillary variable used; however, COK generated similar trends in the spatial variability of Papaver density in all the fields. The cokriged maps are characterized by a higher spatial variation, with several hot spots that are not defined or appreciable in the kriged maps because OK over-smoothed the spatial variability of the primary variable, i.e., Papaver density. The cokriged maps exhibited more local detail and less smoothness in their depiction of the variability of weed density. The spatial distribution maps of weed density produced by COK with ExGR, ExG and ExG(2) vegetation indexes had the best visual resolution compared to those produced using only spatial information (OK) in the five fields.

Assessments of predictions methods

The performance of the COK with wavebands, band ratios and vegetation indexes based on the theoretical fitted models (Table 5) were compared with that of OK in terms of the estimates accuracies. The prediction qualities of the different interpolators were quantitatively compared through the mean-squared prediction error value, the best performing method was

the one that resulted in the lowest MSE. The results in terms of MSE are reported in table 6. The generic geostatistical technique (OK) exhibited the highest MSE value between observed and predicted Papaver density data with an average value of 0.952.

In all the COK approaches the average MSE values decreased, compared to those of ordinary kriging. i.e., the COK interpolation method performed better in all the fields because OK ignored the secondary information and only used the primary weed density variable. The MSE values of COK with G, B/G and R/B of 0.79, 0.78 and 0.80 indicated 17% 18% and 16 % improvements in performance relative to OK, respectively. In general, the MSE values of COK with vegetation indexes were lower and closer to zero than those obtained with COK with wavebands or band ratios, and therefore, COK with vegetation indexes provided the best performance compared to OK. The biggest differences (21.81 %) appeared in Cokriging results with ExGR, followed COK with ExG (21.60 %), ExG(2) (21.48 %), and NGRDI (20.99 %) as covariables (Table 6).

The COK with UAV-derived ancillary variables significantly improved the accuracy of the estimates compared to OK, as shown by the diminished MSE values. It has been emphasized that the potential of multivariate methods to improve OK estimates is high if the associations between the primary and auxiliary variables are robust and important (Simbahan et al. 2006) and that COK results are identical to kriging results when the spatial correlation between the primary and the secondary variables is low or absent (Isaaks and Srivastava 1989; Wackernagel 2003). The results of this study demonstrated that the use of two variables in COK improved the Papaver density predictions compared to OK, even with moderate correlations between the weed density and the secondary variables. These results are in agreement with previous studies by Mutanga and Rugege (2006) who estimated herbaceous biomass using satellite imagery data with COK, and demonstrated that COK is profitable, even in situations previously thought to be impossible due to the weak correlation between the primary and secondary variable. Papritz and Stein (1999) also concluded that the combination of a primary variable with an intensively sampled secondary variable in COK considerably improves the precision of the predictions, since the uncorrelated variations do

not appear in the cross-semivariogram. The good results obtained in this study can be attributed to the capability of COK to utilize the cross-correlation factor between the sparsely sampled Papaver density variable and well-sampled ancillary data derived from high-resolution UAV imagery

Conclusions

The main objective of this work was to investigate if the multivariate geostatistical method of cokriging can be used to improve the accuracy of *Papaver rhoeas* L. infestations maps in winter wheat fields using high-resolution UAV imagery data as secondary variables. This study demonstrated that sparsely samplings of Papaver density in field combined with remotely sensed secondary information obtained from UAV imagery and multivariate geostatistical techniques were adequate to accurately interpolate and map Papaver density in winter wheat crops, when wheat was at the beginning of the maturation stage and showed the typical green-yellow colour and weed patches were at the flowering stage and displayed an intensive red-purple colour.

Cokriging with UAV-derived ancillary variables reduced the errors of interpolation, and therefore, improved the accuracy of weed patches mapping, confirmed by cross-validation. The results have demonstrated that COK with UAV-derived ancillary data is more profitable than other traditional approaches that only incorporate the target weed density variable, e.g., OK (López-Granados et al. 2005; Jurado-Expósito et al. 2009) even in situations when only moderately correlated secondary attributes are available ($r \geq |0.20|$). Although, it is interesting note that the best performances, and therefore, the best resolution of weed infestation maps were obtained when COK was performed with the UAV-derived ancillary variables that yielded the highest correlation with Papaver density, and showed the strongest spatial cross-semivariogram structures. On average, the COK with UAV-derived ancillary variables improved the accuracy of mapping Papaver density by 11 to 21% compared with OK.

In conclusion, it can be said that the multivariate geostatistical method of Cokriging can be used to improve the accuracy of Papaver infestations maps in winter wheat fields

combining sparsely sampled target variable and high-resolution UAV imagery. Although more studies investigating the application of this approach to different weeds and crops, under different cropping and management are required, the COK with UAV-derived ancillary data could be effectively used for accurate herbicide-resistant (or non-resistant) Papaver mapping at late growth stages, e.g., flowering, as a first step towards effective SSWM strategies. In the same way, the approach described by this study could be used to accurately map invasive or herbicide-resistant species that threaten an area and thus helping the development of management strategies. The improved cokriged maps obtained in this study represent useful tools for decision makers to develop appropriate weed control measures or strategies.

The results also suggest the great potential of high-resolution UAV imagery as a source of ancillary information for improving the estimation of sparsely sampled variables using multivariate geostatistics. The need for more and better information to accurately map weed distribution within a field, as a first step towards effective SSWM strategies, can be met by the wider use of UAV platforms and multivariate geostatistics approaches. In this way, the accuracy of maps for precision agriculture could be improved with little additional cost, since the UAV imagery could be obtained as part of other studies. UAVs offer an inexpensive means of providing ancillary variables to estimate sparsely sampled target variables, and therefore a more cost-effective solution to improve the estimation accuracy without intensifying the sampling of the primary variable.

Finally, the good performance of COK to enhance the accuracy of weed maps at late growth stages, e.g., flowering, could be useful to complete or improve other mapping studies at very early phenological stages and then, be used together for developing effective post-emergence SSWM strategies, especially in those cases, such as Papaver, in which the detection and mapping at early phenological stage is complicated.

References

Adjorlolo, C., & Mutanga, O. (2013). Integrating remote sensing and geostatistics to estimate woody vegetation in an African savanna. *Journal of Spatial Science*, 58(2), 305-322.

Barrero, O., & Perdomo, S. A. (2018). RGB and multispectral UAV image fusion for Gramineae weed detection in rice fields. *Precision Agriculture*, doi.org/10.1007/s11119-017-9558-x

Barroso. J., Fernández-Quintanilla, C., Ruiz, D., Hernaiz, P., & Rew, R. J. (2004). Spatial stability of *Avena sterilis* ssp *ludoviciana* populations under annual. *Weed Research*. 44(3), 178–186.

Barroso, J., Ruiz, D., Fernandez-Quintanilla, C., Leguizamon, E. S., Hernaiz, P., Ribeiro, A., Dias, B., Maxwell, B. D., & Rew, L. J. (2005). Comparison of sampling methodologies for site-specific management of *Avena sterilis*. *Weed Research*, 45(2): 165–174.

Blanco-Moreno, J. M., Chamorro, L. & Sans, F. X. (2006). Spatial and temporal patterns of *Lolium rigidum–Avena sterilis* mixed populations in a cereal field. *Weed Research*, 46(3), 207–218.

Bennett, N.D., Croke, B.F.W., Guariso, G., Guillaume, J.H.A., Hamilton, S.H., Jakeman, A.J., et al. (2013). Characterising performance of environmental models. *Environmental Modelling & Software*, 40 (1), 1-20.

Camargo-Neto, J. (2004). A Combined Statistical—Soft Computing Approach for Classification and Mapping Weed Species in Minimum Tillage Systems. Lincoln, NE: University of Nebraska.

Cambardella, C. A., & Karlen, D. L. (1999). Spatial analysis of soil fertility parameters. *Precision Agriculture*, 1(1), 5–11.

Cantero-Martínez, C., Angás, P., Lampurlanés, J. (2007). Long-term yield and water use efficiency under various tillage systems in Mediterranean rainfed conditions. *Annals of Applied Biology*, 150(3), 293–305.

Cardina, J., Jonson, G. A., & Sparrow, D. H. (1997). The nature and consequence of weed spatial distribution. *Weed Science*, 45(3), 364–373.

Castaldi, F., Pelosi, F., Pascucci, S. & Casa, R. (2017). Assessing the potential of images from unmanned aerial vehicles (UAV) to support herbicide patch spraying in maize. *Precision Agriculture*, 18(1), 76-94.

Chilès, J. P., & Delfiner, P. (2012). Geostatistics: modeling spatial uncertainty (2nd ed.). New York: Wiley.

Christensen, S., Søgaard, H.T., Kudsk, P., Nørremark, M., Lund I, Nadimi, S. et al. (2009). Site specific weed control technologies. *Weed Research*, 49(3): 233–241.

Colbach, N., F. Forcella, & Johnson, G. A. (2000). Spatial and temporal stability of weed populations over five years. *Weed Science*, 48(3), 366–377.

Dille, J. A., Milner, M., Groeteke, J. J., Mortensen, D. A., & Williams, M. M. (2003). How good is your weed map? A comparison of spatial interpolators. *Weed Science*, 51(1), 44-55.

De Castro, A. I., Torres-Sánchez, J., Peña, J. M., Jiménez-Brenes, F. M. Csillik, O., & López-Granados, F. (2018). An Automatic Random Forest-OBIA Algorithm for Early Weed Mapping between and within Crop Rows Using UAV Imagery. *Remote Sensing*, 10 (2), 285, doi:10.3390/rs10020285

Donald, W. W. (1994). Geostatistics for mapping weeds, with a Canada thistle (*Cirsium arvense*) patch as a case study. *Weed Science*, 42(4), 648–657.

Everitt, J. H., & Villarreal, R. (1987). Detecting huisache (*Acacia farnesiana*) and mexican palo-verde (*Parkinsonia aculeata*) by aerial photography. *Weed Science*, 35, 427–432.

Emery, X. (2012). Cokriging random fields with means related by known linear combinations. *Computers & Geosciences*, 38(1), 136–144.

Gerhards, R., & Christensen, S. (2006). Site-Specific Weed Management. In A. Srinivasan (Ed.), *Handbook of Precision Agriculture principles and Applications* (pp. 185–206). New York: Food Products Press, The Haworth Press.

Gitelson, A. A., Kaufman, Y. J., Stark, R., & Rundquist, D. (2002). Novel algorithms for remote estimation of vegetation fraction. *Remote Sensing of Environment*, 80(1), 76-87.

Goovaerts, P. (1997). Geostatistics for natural resources evaluation, New York: Oxford University Press, New York Univ. Press.

Goovaerts, P. (2000). Geostatistical approches for incorporating elevation into the spatial interpolation of rainfall. *Journal of Hydrology*, 228(1-2), 113–129.

Heisel, T., Andreasen, C., & Ersbøll, A. K. (1996). Annual weed densities can be mapped with kriging. *Weed Research*, 36(4), 325-337.

Heisel, T., Ersboll, A., & Andreasen, C. (1999). Weed mapping with co-kriging using soil properties. *Precision Agriculture*, 1(1),39-52.

Hernández-Stefanoni, J. L., Gallardo-Cruz, J. A., Meave, J.A., & Dupuy, J.M. (2011). Combining geostatistical models and remotely sensed data to improve tropical tree richness mapping. *Ecological Indicators*, 11(5), 1046–1056.

Hevesi, J. A., Istok, J. D., & Flint, A. L. (1992). Precipitation estimation in mountains terrain using multivariate geostatistics. Part I: structural analysis. *Journal of Applied Meteorology*. 31(1), 661–676.

Holm, L., Doll, J., Holm, E., Pancho, J., & Herbereger, J. (1997). *Papaver rhoeas* L. In: John Wiley and Sons (Ed.), *World Weeds Natural Histories and Distribution* (pp. 555-561). New York: Academic Press.

Huang, Y., Reddy, K. N., Fletcher, R. S., & Pennington, D. (2017). UAV Low-Altitude remote Sensing for Precision Weed Management. *Weed Technology*, doi: 10.1017/wet.2017.89

Isaaks, E. H., & Srivastava, R. M. (1989). An Introduction to Applied Geostatistics. New York: Oxford University.

Izquierdo, J., Blanco-Moreno, J., Chamorro, L., Recasens, J., & Sans, F. (2009). Spatial Distribution and Temporal Stability of Prostrate Knotweed (*Polygonum aviculare*)

and Corn Poppy (*Papaver rhoeas*) Seed Bank in a Cereal Field. *Weed Science*, 57(5), 505-511.

Jordan, C. F. (1969). Derivation of leaf area index from quality of light on the forest floor. *Ecology*, 50(4), 663–666.

Journel, A. y Huijbregts, Ch. (1978). Mining Geostatistics. New York: Academic Press, New York.

Jurado-Expósito, M., López-Granados, F., García-Torres, L., García-Ferrer, A., Sánchez de la Orden, M., & Atenciano, S. (2003). Multi-species weed spatial variability and site-specific management maps in cultivated sunflower. *Weed Science*, 51(3), 319–328.

Jurado-Expósito, M., López-Granados, F., Peña-Barragán, J. M., & García-Torres, L. (2009). A digital elevation model to aid geostatistical mapping of weeds in sunflower crops. *Agronomy for Sustainable Development*, 29(2), 391–400.

Kalivas, D. P., Christos, E. V., Garifalia, E., & Paraskevi, D. (2012). Regional Mapping of Perennial Weeds in Cotton with the Use of Geostatistics. *Weed Science*, 60(2), 233-243.

Kerry, R., & Oliver, M. (2003). Variograms of ancillary data of aid sampling for soil surveys. *Precision Agriculture*, 4(3), 261–278.

Kumar, L., Schmidt, K. S., Dury, S., & Skidmore, A. K. (2001). Imaging spectrometry and vegetation science. In F. van der Meer & S. M. de Jong (Eds.), *Imaging Spectrometry* (pp. 111–155). Dordrecht: Kluwer Academic.

Lambert, J. P. T., Hicks, H. L., Childs, D. Z, & Freckleton, R. P. (2018). Evaluating the potential of Unmanned Aerial Systems for mapping weeds at field scales: a case study with *Alopecurus myosuroides*. *Weed Research*, 58(1), 35–45.

Li, J, & Heap A. D. (2011). A review of comparative studies of spatial interpolation methods in environmental sciences: Performance and impact factors. *Ecological Informatics*, 6, 228–241

López-Granados, F., Jurado-Expósito, M., Peña-Barragán, J. M., & García-Torres, L. (2005). Using geoestatistical and remote sensing approaches for mapping soil properties. *European Journal of Agronomy*, 23(3), 279–289.

López-Granados, F., Torres-Sánchez, J., De Castro, A. I. Serrano-Pérez, A., Mesas-Carrascosa, F. J., & Peña, J. M. (2016). Object-based early monitoring of a grass weed in a grass crop using high resolution UAV imagery. *Agronomy for Sustainable Development.* 36: 67. doi:10.1007/s13593-016-0405-7

Lottes, P., Khanna, R., Pfeifer, J., Siegwart, R., & Stachniss, C. (2017). UAV-based crop and weed classification for smart farming. *IEEE International Conference on Robotics and Automation (ICRA)*, 3024-3031, doi: 10.1109/ICRA.2017.7989347

Matheron, G. (1970). The Theory of Regionalized Variables and Its Applications. Ecole Nationale Supérieure des Mine, 5, 212.

Meng, Q. M., Cieszewski, C., & Madden, M. (2009). Large area forest inventory using Landsat ETM plus: a geostatistical approach. *ISPRS Journal of Photogrammetry and Remote Sensing*, 64(1), 27–36.

Mesas-Carrascosa, F. J., Clavero-Rumbao, I., Torres-Sánchez, J., García-Ferrer, A., Peña, J. M., & López-Granados, F. (2017). Accurate ortho-mosaicked six-band multispectral UAV images as affected by mission planning for precision agriculture proposes. *International Journal of Remote Sensing*, 38 (8–10), 2161–2176.

Mesas-Carrascosa, F. J., Torres-Sánchez, J., Clavero-Rumbao, I., García-Ferrer, A., Peña, J. M., Borra-Serrano, I., & López-Granados, F. (2015). Assessing Optimal Flight Parameters for Generating Accurate Multispectral Orthomosaicks by UAV to Support Site-Specific Crop Management. *Remote Sensing*, 7(10), 12793–12814.

Meyer, G. E., Camargo-Neto, J., Jones, D. D., & Hindman, T. W. (2004). Intensified fuzzy clusters for classifying plant, soil, and residue regions of interest from colour images. *Computers and Electronics in Agri*culture, 42, 161-180.

Mutanga, O., & Rugege, D. (2006). Integrating remote sensing and spatial statistics to model biomass distribution in a tropical savanna. *International Journal of Remote Sensing*, 27(19), 3499–3514.

National Research Council. (1997). Precision Agriculture in the 21st Century: Geospatial and Information Technologies in Crop Management. Washington, DC: National Academy Press.

Oliver, M. A. (2010). Geostatistical Applications for Precision Agriculture . New York, NY: Springer.

Papritz, A., & Stein, A. (1999) Spatial prediction by linear kriging. In A. Stein (Ed.), *Spatial Statistics for Remote Sensing*. Dordrecht: Kluwer.

Peña, J. M., Torres-Sánchez, J., de Castro, A. I., Kelly, M, and López-Granados, F. (2013). Weed mapping in early-season maize fields using object-based analysis of unmanned aerial vehicle (UAV) images. Plos One 8(10), e77151, doi: 10.1371/journal.pone.0077151

Rasmussen, J., Nielsen, J., Garcia-Ruiz, F., Christensen, S., & Streibig, J. C. (2013). Potential uses of small unmanned aircraft systems (UAS) in weed research. *Weed Research*, 53(4), 242–248.

Rouse, J. W., Haas, R. H., Schell, J. A., & Deering, D. W. (1973). Monitoring vegetation systems in the greant plains with ERTS. Proceedings of the Earth Resources Technology Satellite Symposium NASA SP-351, vol 1, (pp. 309–317). Washington, DC.

Schirrmann, M., Hamdorf, A., Giebel, A., Gleiniger, f., Pflanz, M., & Dammer, K. (2017). Regression Kriging for Improving Crop Height Models Fusing Ultra-Sonic Sensing with UAV Imagery. *Remote Sensing*, 9, 665, doi:10.3390/rs9070665

Simbahan, G. C., Dobermann, A., Goovearts, P., Ping, J., & Haddix, M. (2006). Fine resolution mapping of soil organic carbon based on multivariate secondary data. *Geoderma*, 132(3-4), 471–489.

Taberner, A., Anguera, R., Cirujeda, A., & Tarago, R. (2001). Situación actual de las resistencias de *Lolium rigidum* y *Papaver rhoeas* en cereales de invierno. *Phytoma*,132, 33–35.

Thenkabail, P. S., Smith, R. B. & De Pauw, E. (2000). Hyperspectral vegetation indices and their relationships with agricultural crop characteristics. *Remote Sensing of Environment*, 71, 158–182

Torra, J., Cirujeda, A., Taberner, A., & Recasens, J. (2010). Evaluation of herbicides to manage herbicide-resistant corn poppy (*Papaver rhoeas*) in winter cereals. *Crop Protection*, 29(7), 731-736.

Torra, J., Gonzalez-Andujar, J. L., & Recasens, J. (2008). Modelling the population dynamics of *Papaver rhoeas* under various weed management systems in a Mediterranean climate. *Weed Research*, 48(2), 136 -146.

Torra, J., & Recasens, J. (2008). Demography of corn poppy (Papaver rhoeas) in relation to emergence time and crop competition. *Weed Science*, 56(6), 826–833.

Torres-Sánchez, J., López-Granados, F., De Castro, A. I., & Peña-Barragán, J. M. (2013). Configuration and Specifications of an Unmanned Aerial Vehicle (UAV) for Early Site Specific Weed Management. *Plos One*, 8(3), doi:10.1371/journal.pone.0058210

Tucker, C. J. (1977). Asymptotic nature of grass canopy spectral reflectance. *Applied Optics*, 16(5), 1151–1156.

Van der Meer, F. (2012). Remote-sensing image analysis and geostatistics. *International Journal of Remote Sensing*, 33:18, 5644-5676

Wackernagel, H. (2003). Multivariate Geostatistics: an introduction with applications (3rd ed.). Berlin: Springer-Verlag.

Walter, A. M., Christensen, S., & Simmelsgaard, S. E. (2002). Spatial correlation between weed species densities and soil properties. *Weed Research*, 42(1), 26–38.

Webster, R., & Oliver, M. A. (2007). Geostatistics for environmental scientists (2nd ed.). Chichester: John Wiley & Sons, Ltd.

Wilson, B. J., Wright, K. J., Brain, P., Clements, M., & Stephens, E. (1995). Predicting the competitive effects of weed and crop density on weed biomass, weed production and crop yield in wheat. *Weed Research*, 35(4), 265–278.

Woebbecke, D. M., Meyer, G. E., Von Bargen, K., & Mortensen, D. A. (1995). Color indices for weed identification under various soil, residue, and lighting conditions. *Transactions of the ASAE*, 38(1), 259–269.

Yao, H., & Huang, Y. (2013). Remote sensing applications to precision farming. In G. Wang, Q. Weng (Eds.), Remote Sensing of Natural Resources (pp. 333–352). Boca Raton, FL: CRC.

Zhang, N., Wang, M., & Wang, N. (2002). Precision agriculture: a worldwide overview. *Computers and Electronics in Agriculture*, 36(2–3), 113–132.

Zhang, C., & Kovacs, J. (2012). The application of small unmanned aerial systems for precision agriculture: A review. *Precision Agriculture*, 13(6), 693–712.

Table 1 Summary statistics for Papaver density (plants m^{-2}) in Baldomar, Muller, Boix, Cañaveral Norte and Cañaveral Sur

	Fields				
	Baldomar	Boix	Muller	Cañaveral Norte	Cañaveral Sur
Sampled area (ha)	0.42	0.30	0.70	1.00	1.33
n	80	96	110	210	239
Maximum	31	18	32	38	47
Mean	5.360	4.854	4.282	2.967	10.423
Standard deviation	6.346	4.836	5.793	4.889	9.050
Variance	40.276	23.389	33.562	23.898	81.900
Skew	1.748	1.866	2.096	3.464	1.512
Skew (T)	0.002	-0.161	0.274	0.571	-0.399
CV	118.395	99.629	135.300	164.779	86.827
CV (T)	79.865	70.998	89.956	106.53	39.641

n: number of georeferenced sampling sites

Skew (T): skewness of log-transformed variable after adding a constant value of 1

CV: coefficient of variation (%)

CV: coefficient of variation (%) of log-transformed variable after adding a constant value of 1

Table 2 Ancillary variables derived from UAV imagery used in the multivariate geostatistical method of cokriging

Secondary variable			Reference
Waveband	Red	R	
	Green	G	
	Blue	B	
	Near-infrared	NIR	
Band ratio	Blue/Green	B/G	
	Red/Green	R/G	
	R/B index	R/B	Everitt and Villarreal 1987
	Near-infrared/Green	NIR/G	
Vegetation Index	Ratio Vegetation Index	RVI	Jordan 1969
	Normalised Difference Vegetation Index	NDVI	Rouse et al. 1973
	Difference Vegetation Index	DVI	Jordan 1969
	Excess Green Index	ExG	Woebbecke et al. 1995
	Normalised Green-Red Difference Index	NGRDI	Gitelson et al.2002
	Normalised Excess Green Index	ExG(2)	Woebbecke et al. 1995
	Excess Red Index	ExR	Meyer et al. 2004
	Normalised Excess Red Index	ExR(2)	Meyer et al. 2004
	Excess Green minus Excess Red Index	ExGR	Camargo-Neto 2004

Table 3 Relationship between Papaver density and UAV-derived ancillary variables

		Field				
		Baldomar	**Boix**	**Muller**	**Cañaveral**	**Cañaveral**
Ancillary variable					**Norte**	**Sur**
Waveband	R	-0.287*	0.285*	0.192ns	-0.318*	-0.373*
	G	-0.519**	0.508**	0.492*	-0.501**	-0.471**
	B	0.200*	0.256*	0.292*	-0.317*	-0.381*
	NIR	-0.029ns	-0.083ns	0.107ns	0.126ns	0.181ns
Band ratio	B/G	-0.601**	0.593**	0.510**	-0.607**	-0.606**
	R/G	0.340*	0.321*	-0.212*	-0.498*	-0.191ns
	R/B	0.396*	-0.307*	-0.206*	0.420*	-0.429*
	NIR/G	-0.121ns	-0.159ns	0.186ns	0.188ns	0.193ns
Vegetation Index	RVI	0.108ns	-0.026ns	0.034ns	0.161ns	0.161ns
	NDVI	0.121ns	-0.034ns	0.010ns	0.122ns	0.156ns
	DVI	-0.071ns	-0.085ns	0.072ns	0.131ns	0.193ns
	ExG	-0.632**	-0.607**	0.523**	0.657**	0.677**
	NGRDI	-0.428*	-0.414*	0.310*	0.502**	0.426*
	ExG(2)	-0.603**	-0.621**	0.504**	0.611**	0.631**
	ExR	-0.447*	0.481*	0.301*	-0.436*	-0.484*
	ExR(2)	0.429*	0.450*	-0.314*	-0.482*	0.475*
	ExGR	0.604**	-0.621**	0.508**	0.616**	0.608**

Secondary variables: R: Red; G: Green; B: Blue; NIR: Near-infrared. RVI: Ratio Vegetation Index; NDVI: Normalised Difference Vegetation Index; DVI: Difference Vegetation Index; ExG: Excess Green Index; NGRDI: Normalised Green-Red Difference Index; ExG(2): Normalised Excess Green; ExR: Excess Red Index; ExR(2): Normalised Excess Red and ExGR: Excess Green minus Excess Red, ExGR

*Significance level: p>0.5

**Signifcance level: p>0.01

ns: not significance

Table 4 Results of fitted semivariogram models and spatial distribution characteristics of Papaver for using in the ordinary kriging interpolation method

Field	Model	Semivariograms parameters				Spatial class	Cross-validation statistics			
		Nugget	Range (m)	Sill	SD (%)		MEE	MSE	SMSE	Variance Error
Baldomar	Exponential	0.00	30.74	1.23	0.00	S	0.0050	0.9702	0.9302	0.7728
Boix	Exponential	0.00	15.44	1.04	0.00	S	-0.0096	0.9222	0.9777	0.7511
Muller	Exponential	0.37	18.46	0.78	47.52	M	0.0103	0.9806	0.9943	0.9202
Cañaveral Norte	Exponential	0.00	22.76	0.76	0.00	S	0.0100	0.9579	0.9902	0.4340
Cañaveral Sur	Exponential	0.00	23.16	0.65	0.00	S	0.0018	0.9329	0.9970	0.4022

SD: Spatial Dependence index: Nugget ratio (%) = (nugget semivariance/ total semivariance)* 100

Spatial class: S= strong spatial dependence; M= moderate spatial dependence

MEE: mean estimation error; MSE: mean squared error; SMSE: standardized mean squared error

Table 5 Results of fitted cross-semivariogram exponential models for using in the cokriging interpolation methods

Field	Secondary variable				Cross-validation statistics			
		Nugget	Range	Sill	MEE	MSE	SMSE	Variance error
Baldomar	G	0.08	32.30	1.13	0.0009	0.850	0.953	0.807
	B/G	0.08	32.30	1.13	0.0025	0.849	0.931	0.883
	R/B	0.00	30.74	1.23	0.0032	0.852	0.934	0.781
	ExG	0.27	43.07	0.98	0.0044	0.809	0.949	0.811
	NGRDI	0.08	32.30	1.13	0.0060	0.814	0.944	0.798
	ExG(2)	0.26	45.79	1.05	0.0065	0.803	0.933	0.778
	ExR	0.00	25.84	1.18	-0.0023	0.821	0.930	0.811
	ExR(2)	0.08	34.10	1.13	0.0068	0.828	0.948	0.791
	ExGR	0.28	41.79	1.02	0.0065	0.807	0.935	0.781
Boix	G	0.01	14.82	1.01	-0.0064	0.854	0.975	0.752
	B/G	0.00	14.82	1.02	-0.0049	0.836	0.959	0.707
	R/B	0.01	14.16	1.01	-0.0087	0.861	0.972	0.750
	ExG	0.00	15.46	1.04	-0.0042	0.822	0.970	0.716
	NGRDI	0.35	19.10	0.64	0.0047	0.829	0.995	0.802
	ExG(2)	0.00	14.16	0.92	-0.0016	0.826	0.973	0.724
	ExR	0.05	13.49	0.92	0.0056	0.820	0.993	0.765
	ExR(2)	0.05	14.71	0.96	-0.0038	0.826	0.981	0.740
	ExGR	0.00	15.82	0.87	-0.0013	0.818	0.978	0.728
Muller	G	0.00	11.73	1.11	0.0179	0.953	0.950	0.917
	B/G	0.00	12.77	1.14	0.0187	0.942	0.975	0.997
	R/B	0.28	15.54	0.85	0.0144	0.990	0.989	1.022
	ExG	0.27	17.68	0.91	0.0068	0.916	0.986	0.981
	NGRDI	0.00	12.18	1.12	0.0189	0.927	0.970	0.984
	ExG(2)	0.03	12.89	1.14	0.0181	0.929	0.975	0.987
	ExR	0.01	13.19	1.14	0.0165	0.939	0.983	1.007
	ExR(2)	0.00	12.89	0.98	0.0158	0.934	0.960	0.938
	ExGR	0.00	12.22	1.09	0.0178	0.910	0.975	0.969
Cañaveral	G	0.00	21.97	0.77	0.0091	0.663	0.892	0.441
Norte	B/G	0.12	27.02	0.65	0.0117	0.646	0.940	0.459
	R/B	0.01	22.34	0.73	0.0107	0.668	0.928	0.449
	ExG	0.34	92.96	0.65	0.0019	0.610	0.931	0.465
	NGRDI	0.22	38.22	0.63	0.0035	0.621	0.886	0.439
	ExG(2)	0.24	43.46	0.64	0.0051	0.611	0.885	0.438
	ExR	0.32	60.44	0.54	0.0057	0.630	0.931	0.479
	ExR(2)	0.20	35.74	0.63	0.0034	0.639	0.890	0.436
	ExGR	0.25	44.44	0.63	0.0040	0.611	0.884	0.439
Cañaveral	G	0.13	29.48	0.50	0.0042	0.656	1.005	0.433
Sur	B/G	0.03	23.23	0.59	0.0024	0.673	1.005	0.415
	R/B	0.00	22.15	0.62	0.0038	0.656	0.988	0.436
	ExG	0.00	19.66	0.64	0.0008	0.608	0.961	0.422
	NGRDI	0.00	18.00	0.62	-0.0006	0.603	0.975	0.442
	ExG(2)	0.00	20.14	0.60	0.0012	0.602	0.978	0.401
	ExR	0.03	23.37	0.58	0.0024	0.616	0.989	0.407
	ExR(2)	0.04	24.23	0.57	0.0025	0.617	1.046	0.434
	ExGR	0.00	20.60	0.59	0.0007	0.608	0.994	0.422

MEE: mean estimation error, MSE: mean squared error, SMSE: standardized mean squared error

Table 6 Average performances of ordinary kriging and cokriging predictions methods for Papaver estimation

Prediction method	Secondary variable		MSE	Improvement by Cokriging*
OK			0.9527	
COK	Waveband	G	0.7958	17.18
	Band ratio	B/G	0.7816	18.66
		R/G	0.7934	17.43
		R/B	0.8041	16.32
	Vegetation index	ExG	0.7533	21.60
		NGRDI	0.7592	20.99
		ExG(2)	0.7544	21.48
		ExR	0.7657	20.31
		ExR(2)	0.7689	19.97
		ExGR	0.7513	21.81

MSE: mean squared error, average value of the five fields studied

Secondary variables: R: Red; G: Green; B: Blue; ExG: Excess Green Index; NGRDI: Normalised Green-Red Difference Index; ExG(2): Normalised Excess Green; ExR: Excess Red Index; ExR(2): Normalised Excess Red and ExGR: Excess Green minus Excess Red, ExGR

*Improvement in performance relative to OK (%)

Fig. 1 UAV multispectral ortho-mosaicked images of the whole experimental fields. Black dots and red squares indicate the position of the georeferenced sampled points and the ground control poinst (GCP) used in the study, respectively.

(a) Baldomar

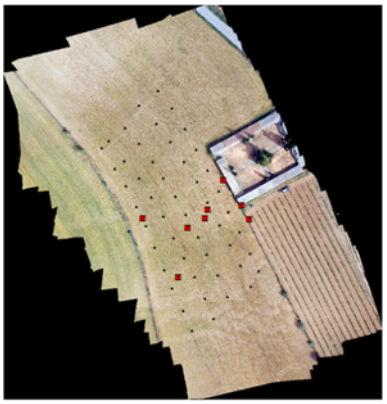

(b) Boix

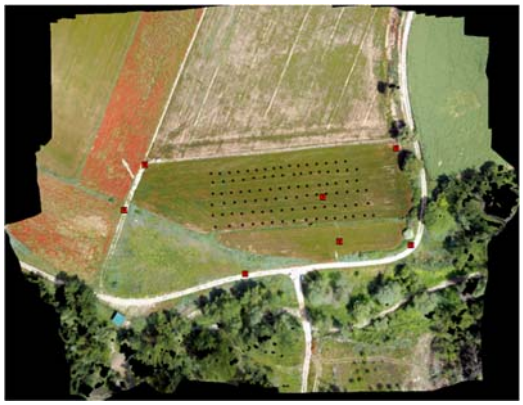

(c) Muller

(d) Cañaveral Norte

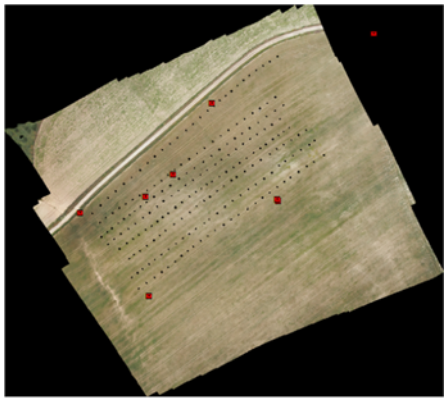

(e) Cañaveral Sur

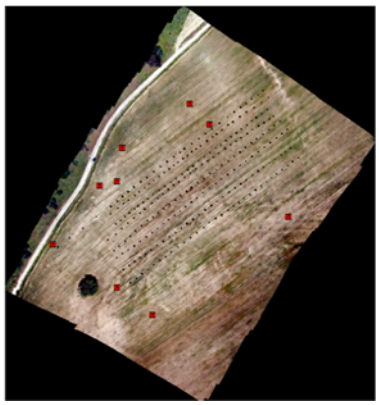

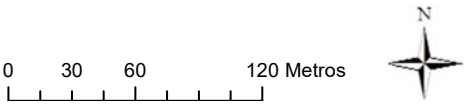

Fig. 2 Experimental semivariograms (+) and fitted models (-) of Papaver used in the ordinary kriging interpolation method; h is distance in metres and Ɣ is the semivariance values

(a) Baldomar

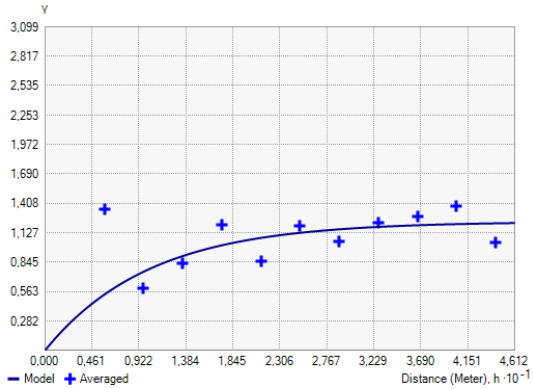

(b) Boix

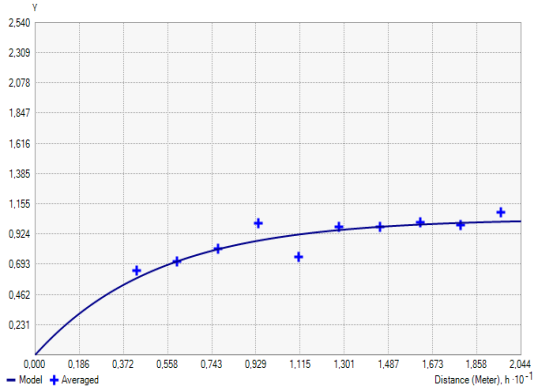

(c) Muller

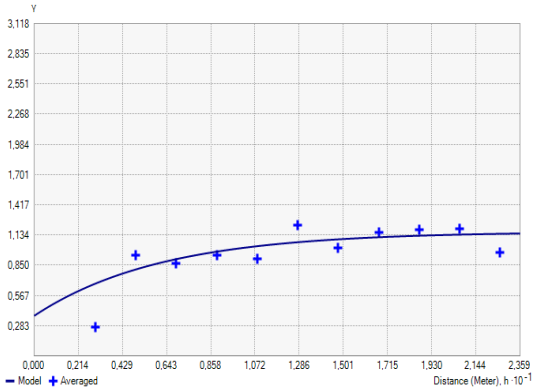

(d) Cañaveral Norte

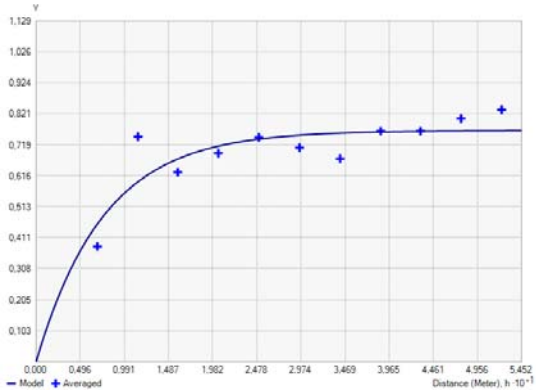

(e) Cañaveral Sur

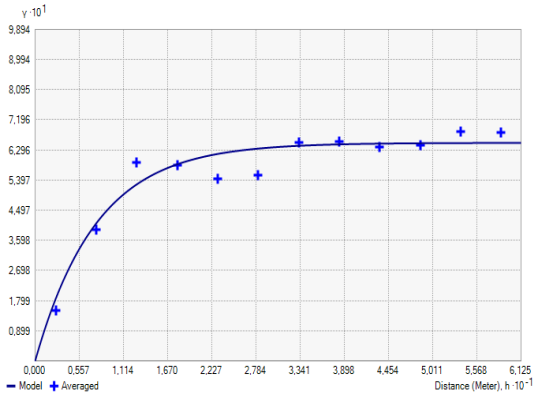

Fig. 3 Experimental cross-semivariograms (+) and fitted models (-) between Papaver and UAV-derived ancillary variables used in the cokriging interpolation method; h is distance in metres and ϒ is the semivariance values

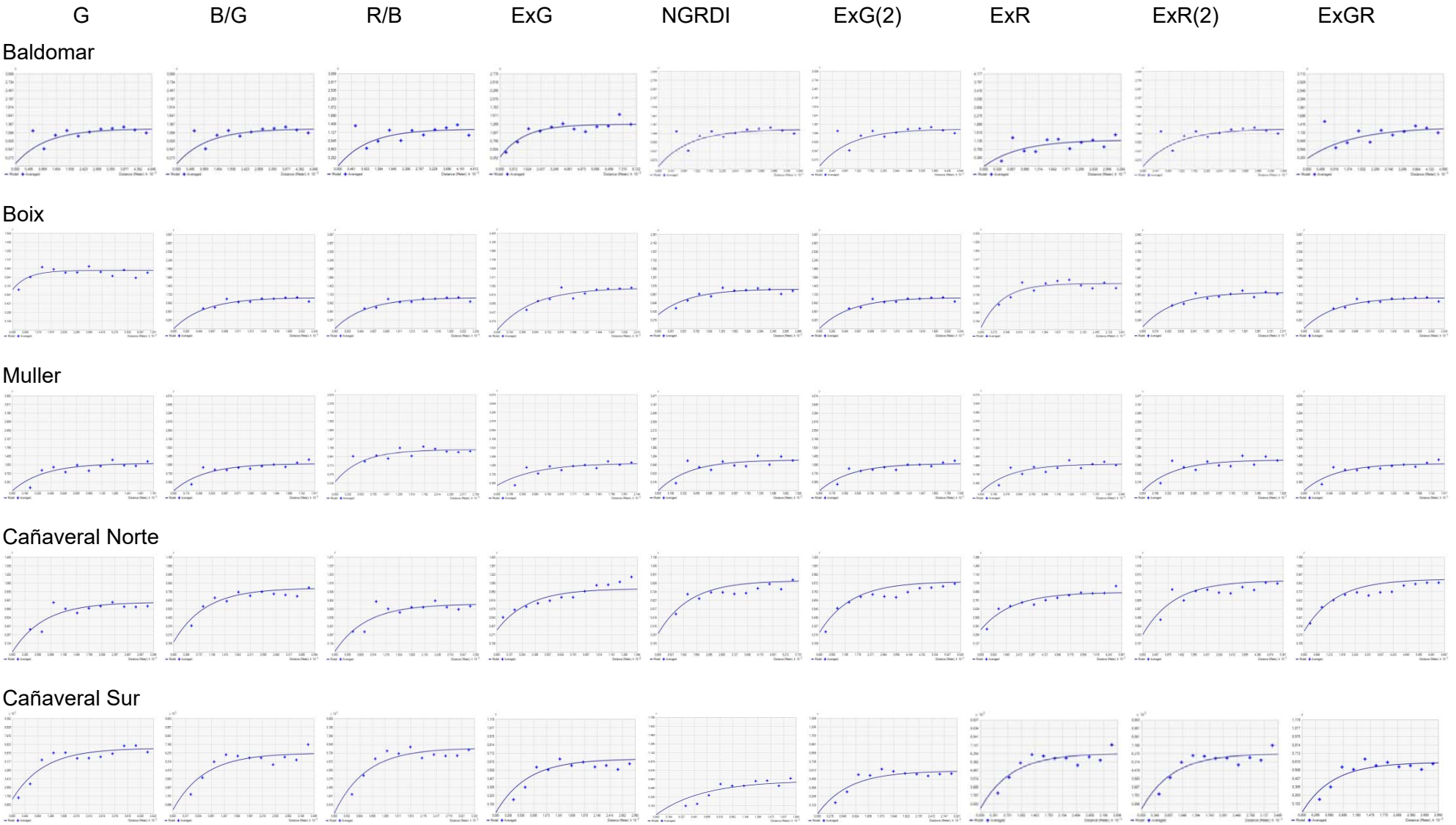

Fig. 4 Spatial distribution of Papaver using the ordinary kriging interpolation method

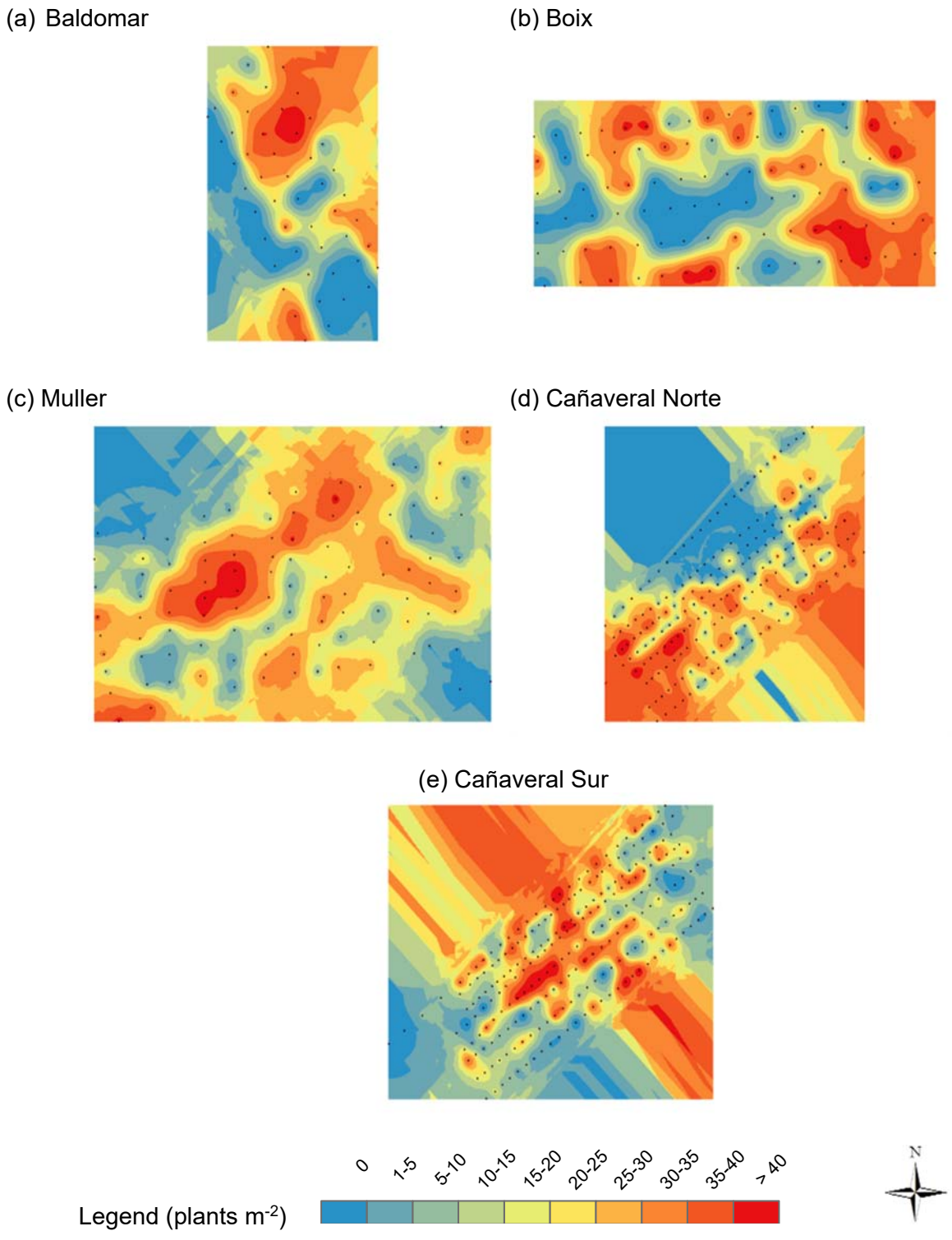

Fig. 5 Spatial distribution of Papaver using the cokriging with UAV-derived ancillary variables interpolation methods